

# Steady-State Oscillations in Resonant Electrostatic Vibration Energy Harvesters

Elena Blokhina, *Member, IEEE*, Dimitri Galayko, *Member, IEEE*, Philippe Basset, and Orla Feely, *Fellow, IEEE*

**Abstract**—In this paper, we present a formal analysis and description of the steady-state behavior of an electrostatic vibration energy harvester operating in constant-charge mode and using different types of electromechanical transducers. The method predicts parameter values required to start oscillations, allows a study of the dynamics of the transient process, and provides a rigorous description of the system, necessary for further investigation of the related nonlinear phenomena and for the optimisation of converted power. We show how the system can be presented as a nonlinear oscillator and be analysed by the multiple scales method, a type of perturbation technique. We analyse two the most common cases of the transducer geometry and find the amplitude and the phase of steady-state oscillations as functions of parameters. The analytical predictions are shown to be in good agreement with the results obtained by behavioral modeling.

**Index Terms**—Bifurcation analysis, electrostatic vibration energy harvesters, multiple scale method, steady-state oscillations.

## I. INTRODUCTION

**E**LECTROSTATIC (capacitive) vibration energy harvesters (e-VEHs) convert kinetic energy of the environment into electrical energy using a capacitive transducer [1]. E-VEHs are particularly suitable for microscale implementation and have become in recent years the subject of a growing area of research [2]–[11]. The main issue of e-VEH design is the optimization of converted power for given environmental conditions and given limitations of the electrical and mechanical components [12]. This optimisation requires a tool estimating the converted power for a given set of design parameters and operation conditions [13], [14]. To date, such a tool is still lacking. The architecture and operation of VEHs based on electrostatic transducers is intrinsically more complex than for the case of electromagnetic and piezoelectric VEHs [4], [15]–[17]. Because of periodic charge/discharge cycles, the system is time-variant and cannot be adequately analysed with a simple analytical approach such as linearization around an operating point. The conditioning circuit brings additional complexity to the system since its architecture and operating

mode impact directly the mechanical dynamics of the resonator. For these reasons, an optimal design of an e-VEH requires a deep understanding of the overall system dynamics, including nonlinear effects.

There are practical reasons for developing a theoretical analysis. It allows the prediction and analysis of irregular and chaotic behavior for realistic configurations of the conditioning circuit as highlighted in [18]. As a result, one can bound the area of internal and external parameters of the system where stable harmonic vibrations exist. Based on that knowledge, one can predict the most effective operating parameters of the e-VEH (such as the amplitude of the mobile mass displacement) at the design stage, and thereby optimise converted power.

Indeed, most existing conditioning circuits for e-VEHs [2], [4], [5], [8] operate correctly only in the context of regular quasi-sinusoidal motion of the resonator, since their operating mode is based on the detection of the maximum and minimum of the transducer capacitance. Theoretically, in a non-regular mode there can be a large number of local maxima and minima during a particular time interval (e.g., during one period of the external vibration). In practice, the dynamics of the system over these intervals are defined by non-idealities of the conditioning circuit (for example, there is always a delay in the detection of extrema in realistic circuits) and are virtually impossible to predict. Such irregular behavior is not compatible with an optimal operating mode of the e-VEH system, and the designer of the e-VEH must avoid such regimes. Hence, the theory should allow the analysis of irregular modes and clearly indicate the limits between regular and irregular behavior.

The work [14] has suggested a general analytical tool for analysis of a resonant electrostatic VEH operating in the mode of strong electro-mechanical coupling. The tool proposed there introduces the amplitude-dependent mechanical impedance of the nonlinear system “conditioning circuit—capacitive transducer” that allows one to use a well-known method of analysis of electrical networks. This tool is comprehensive for those who are familiar with electronic design tools, and it provides a good agreement with behavioral modeling. However, this tool is still limited for further exploration of non-regular behavior and does not take into account the eventual zero-frequency shift of the mobile mass position, which can be significant for transducers with asymmetric geometry (typically, a gap-closing transducer).

Building on this work, our paper presents a formal approach based on the application of the multiple scales method (MSM) to a resonant e-VEH with the most common conditioning circuit proposed in [4]. In this approach, the system is presented as a nonlinear oscillator where the electromechanical transducer generates a nonlinear force. With this conditioning circuit, the

Manuscript received April 24, 2012; accepted June 18, 2012. This work was supported by Science Foundation Ireland and by the French National Agency of Research through the contract ANR-08-SEGI-019. This paper was recommended by Associate Editor H. S. Chung.

E. Blokhina and O. Feely are with the School of Electrical, Electronic and Communications Engineering, University College Dublin, Belfield, Dublin 4, Ireland (e-mail: elena.blokhina@ucd.ie; orla.feely@ucd.ie).

D. Galayko is with LIP6, UPMC—Sorbonne Universités, 75005 Paris, France (e-mail: dimitri.galayko@lip6.fr).

P. Basset is with Université Paris-Est, ESYCOM, ESIEE Paris, BP 99 93162 Noisy-le-Grand Cedex, France (e-mail: p.basset@esiee.fr).

Digital Object Identifier 10.1109/TCSI.2012.2209295

transducer operates in a constant-charge triangular QV energy conversion cycle that is considered as being the most efficient mode of operation [19]. Like the tool in [14], the proposed method allows one to find parameters of steady-state oscillations (such as the amplitude and phase) as functions of parameters of the conditioning circuit, the resonator and the external acceleration. In addition, the MSM provides a straightforward route for bifurcation and stability analysis and for the analysis of transient process, and it can easily be adjusted for different types of nonlinearities such as nonlinear air damping, mechanical (spring) nonlinearity and different forms of the transducer force. In particular, the analysis presented here predicts analytically the irregular behavior of the eVEH at weak amplitudes discovered previously by simulations in a behavioral model [18].

The validation of the analytical results is carried out by employing mixed VHDL—AMS/Eldo simulations of the e-VEH described in detail in [14]. Two VHDL-AMS/Eldo models are considered. The first one is a simplified model that implements an ideal operating regime of a capacitive transducer in constant-charge mode. The second model implements the conditioning circuit described in [4] and takes into account certain effects typical for realistic systems such as losses in diodes and finite charging times of the variable capacitors. Our analysis and simulations are carried out for two types of transducer: a gap-closing transducer whose capacitance is a hyperbolic function of the displacement and an area overlap transducer whose capacitance is a linear function of the displacement.

The paper is organised as follows. In Section II we discuss the architecture of the system and its governing equations. Section III describes the behavioral VHDL-AMS/Eldo models of the e-VEH. Section IV presents the MSM-based analysis of the system while and Section V gives the results of the application of the MSM methods to transducers with the two geometries and discusses the comparison between the simulations and analytical results.

## II. STATEMENT OF THE PROBLEM

In this section, we introduce the electromechanical model used to describe our VEH devices. A simple electrostatic harvester consists of a resonator, a variable capacitor (a transducer)  $C_{\text{tran}}$  and a conditioning circuit (Fig. 1). The resonator frame moves due to the external vibrations. The displacement  $x$  of the mobile mass with respect to the frame is also affected by the transducer force  $f_t$ . Therefore, the equation defining  $x$  is

$$\ddot{x} + (b/m)\dot{x} + \omega_0^2 x = A_{\text{ext}} \cos(\omega_{\text{ext}} t + \vartheta_0) + f_t/m \quad (1)$$

where  $m$  is the mass of the resonator,  $b$  is the damping factor,  $\omega_0 = \sqrt{k/m}$  is the natural frequency,  $k$  is the spring constant,  $A_{\text{ext}}$  is the acceleration amplitude of external vibrations,  $\omega_{\text{ext}}$  is the external frequency and  $\vartheta_0$  is the initial phase of the external vibrations.

The transducer force  $f_t$  depends on the transducer voltage  $V_{\text{tran}}$  and on the mobile mass position  $x$ :

$$f_t(x, V_{\text{tran}}) = \frac{V_{\text{tran}}^2}{2} \frac{dC_{\text{tran}}}{dx} \quad (2)$$

where  $V_{\text{tran}}$  is generated by the conditioning circuit from Fig. 1 proposed in [4] that implements the constant-charge

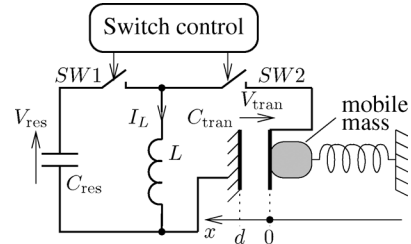


Fig. 1. Schematic view of an electrostatic vibration energy harvester implementing the constant-charge triangular QV energy conversion cycle [4].

triangular QV energy conversion cycle. The conditioning circuit discharges the transducer to zero when the transducer capacitance is at a local minimum and charges it to a charge  $Q_0$  when its capacitance is at a local maximum. The energy conversion is achieved when the transducer capacitance decreases keeping its charge constant ( $Q_0$ ). During this process, mechanical energy is converted into electrical energy, and the transducer acts as a damper in the mechanical domain. In the case of transducers with monotonously increasing  $C_{\text{tran}}(x)$  characteristics, the voltage generated by the transducer depends on the sign of the mobile mass velocity:  $V_{\text{tran}} = 0$  if  $\dot{x} > 0$  and  $V_{\text{tran}} = Q_0 C_{\text{tran}}(x(t))$  if  $\dot{x} < 0$ . Hence, the force is a piecewise defined function:  $f_t = 0$  if  $\dot{x} > 0$  and  $f_t = f_t(x, Q_0/C_{\text{tran}}(x))$  otherwise, and will be referred later as  $f_t(x, \dot{x})$ .

At a *local maximum* of  $C_{\text{tran}}$ , the conditioning circuit fixes three electrical quantities on the transducer: the charge  $Q_0$ , the voltage  $V_0$  and the energy  $W_0$ . Only one of the three can be fixed independently from the others since they are related by the following expressions:

$$Q_0 = C_{\text{max}} V_0, \quad W_0 = \frac{1}{2} \frac{Q_0^2}{C_{\text{max}}}. \quad (3)$$

Here  $C_{\text{max}}$  is the local maximum value of the  $C_{\text{tran}}$ . It is important to understand that  $C_{\text{max}}$  is a dynamic quantity which may change at each local maximum of  $C_{\text{tran}}$  and which is constant during the time intervals between two consecutive local maxima.  $C_{\text{max}}$  is constant in a steady-state harmonic mode.

At a *local minimum* the three quantities are set to zero. The quantity (one from the three) that is independently fixed to a non-zero value at a local maximum depends on the architecture of the conditioning circuit. In this paper, we consider the most common case valid for the circuit in Fig. 1 where the energy  $W_0$  is fixed [4] (see the description of the behavioral model in Section III).

Whatever quantity is fixed on the transducer at a local maximum of  $C_{\text{tran}}$ , the charge  $Q_0$  does not change until the next local minimum of  $C_{\text{tran}}$  is reached. The electromechanical energy conversion is carried out during the time interval corresponding to the motion of the mobile plate from  $C_{\text{max}}$  to  $C_{\text{min}}$  positions. This energy conversion mode is called in literature the *constant-charge operating mode* of the transducer, which underlines the fact the transducer keeps a constant electrical charge during the electrical energy generation.

For an area overlap transducer [20], the capacitance is  $C_{\text{tran}} = C_0 + \alpha_{\text{tran}} x$  and  $V_{\text{tran}} = Q_0/C_{\text{tran}} =$

$\sqrt{2W_0C_{\max}}/C_{\text{tran}}$ . The expression for the transducer force in this case is

$$f_{t,1}(x, \dot{x}) = \begin{cases} \frac{W_0\alpha_{\text{tran}}(1 + \alpha_{\text{tran}}x_{\max}/C_0)}{C_0(1 + \alpha_{\text{tran}}x/C_0)^2}, & v \leq 0 \\ 0 & v > 0 \end{cases} \quad (4)$$

Here  $x_{\max}$  is the local maximum of  $x$ , defined similarly to  $C_{\max}$ .

In order to reduce the number of parameters and outline only essential ones, the following normalised variables are introduced: time  $\tau = \omega_0 t$ , dissipation  $\beta = b/(2m\omega_0)$ , normalised external vibration frequency  $\Omega = \omega_{\text{ext}}/\omega_0$ ,  $y = \alpha_{\text{tran}}x/C_0$ ,  $\alpha = \alpha_{\text{tran}}A_{\text{ext}}/(C_0\omega_0^2)$  and  $\kappa_0 = \alpha_{\text{tran}}^2W_0/(C_0^2m\omega_0^2)$ . Equation (1) is now written as

$$y'' + 2\beta y' + y = f_t(y, y') + \alpha \cos(\Omega\tau + \theta_0) \quad (5)$$

where the prime denotes the derivative with respect to dimensionless time  $\tau$  and the function  $f_t(y, y')$  is the normalised version of (4):

$$f_{t,1}(y, y') = \begin{cases} \frac{\kappa_0(1+y_{\max})}{(1+y)^2}, & y' \leq 0 \\ 0 & y' > 0 \end{cases} \quad (6)$$

The same (5) may be used to describe the system with other types of transducers. For the transducer with hyperbolic capacitance function [14], [18]  $C_{\text{tran}}(x) = C_0/(1 - x/d)$ , the transducer force is

$$f_{t,2}(x, v) = \begin{cases} \frac{W_0}{d(1-x_{\max}/d)}, & v \leq 0 \\ 0 & v > 0 \end{cases} \quad (7)$$

Here  $d$  is the transducer gap at rest ( $f_{\text{tran}} = 0$  and  $A_{\text{ext}} = 0$ ) and  $x_{\max}$  is the maximum value of displacement  $x$ . Introducing the variables and parameters  $y = x/d$ ,  $\alpha = A_{\text{ext}}/(d\omega_0^2)$  and  $\nu_0 = W_0/(d^2m\omega_0^2)$ , one obtains the force in the form

$$f_{t,2}(y, y') = \begin{cases} \frac{\nu_0}{(1-y_{\max})}, & y' \leq 0 \\ 0 & y' > 0 \end{cases} \quad (8)$$

In this study, we consider the geometry of the transducers and resonator as fixed (the mass, the natural frequency and the transducer dimensions are constant), whereas the external acceleration amplitude  $A_{\text{ext}}$  and the energy  $W_0$  are the design parameters which may vary and affect the behavior of the system. By consequence, for the normalised equation, there are two control parameters of the dynamical system:  $\alpha$  and  $\kappa_0$  for area overlap transducer and  $\alpha$  and  $\nu_0$  for gap-closing transducer.

Numerical examples will be presented with typical parameters of systems (4) and (7), as given in Table I. The values are taken from [14] and [16].

### III. BEHAVIORAL MODELING OF THE E-VEH

The modeling of the e-VEH has been carried out employing a mixed SPICE and behavioral description implemented in the VHDL-AMS/Eldo environment provided with the AdvanceMS tool of Mentor Graphics. The conditioning circuit is implemented as an electrical network described by an Eldo netlist (Eldo is a commercial variant of the SPICE simulator). The transducer and resonator are described by a VHDL-AMS

TABLE I  
PARAMETERS OF THE SYSTEMS

	Area overlap	hyperbolic
m	$50 \cdot 10^{-6}$ kg	$200 \cdot 10^{-6}$ kg
b	$2.16 \cdot 10^{-3}$ Nsm $^{-1}$	$\sqrt{2} \cdot 10^{-3}$ Nsm $^{-1}$
k	$150$ Nm $^{-1}$	$300$ Nm $^{-1}$
d	—	$20 \cdot 10^{-6}$ m
S	—	$10 \cdot 10^{-4}$ m $^2$
$\alpha_{\text{tran}}$	$10^{-6}$ Fm $^{-1}$	—
$C_0$	$150 \cdot 10^{-12}$ F	—
L	$3 \cdot 10^{-3}$ H	—
$W_0$	$< 10 \cdot 10^{-8}$ J	$< 3 \cdot 10^{-8}$ J
$A_{\text{ext}}$	$< 30$ ms $^{-2}$	$< 10$ ms $^{-2}$

model. We consider two models that have different implementations of the condition circuit from Fig. 1. The first model employs an ideal simple circuit and the second model employs a circuit that includes certain ‘nonidealities’ that can be found in realistic circuits.

#### A. VHDL-AMS Model of the Transducer/Resonator

The VHDL-AMS language is a powerful tool that allows one to describe physical systems defined by lumped-parameter differential equations. This language is particularly suitable for the description of behavior of systems interfaced with electrical networks [21]. A VHDL-AMS model of the transducer/resonator block can be seen as an electrical dipole behaving as a variable capacitor. The capacitance variation is obtained through resolution of Newtonian equations written for the resonator which also takes into account the force  $f_t$  generated by the transducer. Presented in [18], the VHDL-AMS model of the transducer/resonator block is a system of physical differential equations:

$$\begin{aligned} f_t &= \frac{1}{2}V_{\text{tran}}^2 \frac{\partial C_{\text{tran}}}{\partial x}, \quad C_{\text{tran}} = C_{\text{tran}}(x), \\ -kx - \mu\dot{x} + f_t &= m\ddot{x} - ma_{\text{ext}}(t), \\ i &= \dot{q}, \\ q &= C_{\text{tran}}V_{\text{tran}}. \end{aligned} \quad (9)$$

Here  $a_{\text{ext}}(t)$  is the known acceleration of the external vibrations,  $q$ ,  $i$  and  $v$  are the charge, current and voltage through the terminals of the variable transducer capacitor. The model solves these five equations for five unknown quantities:  $f_t$ ,  $x$ ,  $q$ ,  $C_{\text{tran}}$  and  $i$  or  $v$ . One of the two latter quantities or a relation between them is defined by the electrical network connected to the modeled dipole.

#### B. Mixed VHDL-AMS/Eldo Model of the Conditioning Circuit

In order to formally validate the theory presented in the paper, we used the conditioning circuit model shown in Fig. 2. Its goal is to create an electrical context for the transducer that exactly corresponds to the constant-charge energy conversion regime described by the equations given in Section II [4]. The switches SW1 and SW2 are driven by short pulses corresponding to the moments of local maxima and minima of  $C_{\text{tran}}$ . These pulses are long enough to charge the transducer at a local maximum of  $C_{\text{tran}}$  to  $V_0$  and to discharge it through a small load resistance when  $C_{\text{tran}}$  reaches a local minimum. The voltage  $V_0$  is defined as a function of the value of the local maximum of  $C_{\text{tran}}$  through the formula  $W_0 = V_0^2C_{\max}/2$ , where  $W_0$  is a constant

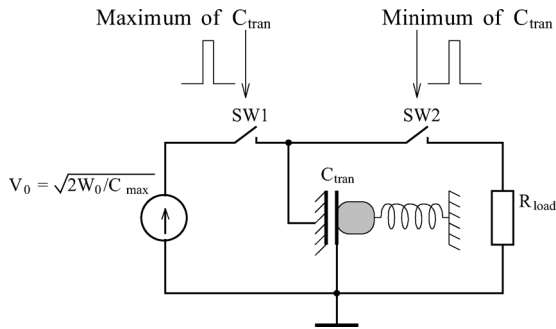


Fig. 2. Simplified idealised conditioning circuit.

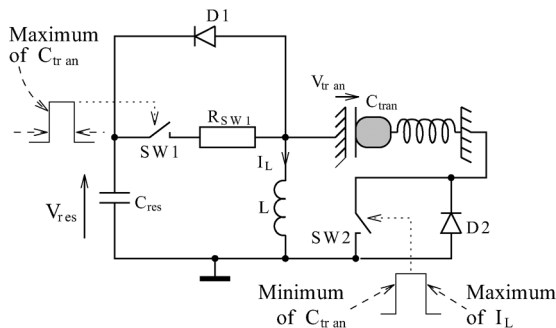


Fig. 3. Model of the realistic conditioning circuit.

parameter of the model. This model emulates the ideal electrical environment for a transducer operating in constant-charge mode and requires few resources for simulations. It is not realistic and is only used for the intermediate theory validation.

A more realistic model of the conditioning circuit is given in Fig. 3. It is directly based on the circuit presented in [4]. Initially, the large reservoir capacitor  $C_{res}$  is charged up to some voltage  $V_{res}$  that is assumed to be constant since  $C_{res}$  is large. The model is provided with blocks described in VHDL-AMS allowing the detection of a local maximum and minimum of  $C_{tran}$  and of a local maximum of the inductor current  $I_L$ .

When a local maximum of  $C_{tran}$  is detected, the switch SW1 is closed for a fixed time  $\tau$ , thus loading the inductor to a current

$$I_L = \frac{\tau V_{res}}{L}. \quad (10)$$

The corresponding energy of the inductor is

$$W_0 = LI_L^2/2. \quad (11)$$

After the time  $\tau$ , SW1 is open and the inductor current flows through the diode  $D2$  and charges  $C_{tran}$  (forward charge transfer). Note that whatever the value of  $C_{tran}$  is at that moment, the inductor gives it the energy  $W_0$  that is a free design parameter of this architecture and is uniquely related with  $L$ ,  $V_{res}$  and  $\tau$ .

Both processes (the inductor and capacitor charging) are very fast and they take place during a time that is negligible with respect to the variation period of  $C_{tran}$ . This is ensured by the appropriate choice of the value of the inductance  $L$ .

After that, both switches are closed, and the electrostatic transducer operates in constant-charge mode. When  $C_{tran}$

 TABLE II  
PARAMETERS OF VHDL-AMS/ELDO MODELS

Parameter name	Value
$C_{res}$	10 $\mu\text{F}$
$R_{SW1}, R_{load}$	0.001 $\Omega$
$W_0$	
for the gap-closing transducer:	15...25 nJ
for the area overlap transducer:	10...100 nJ
$L$	10 mH
$V_{res}$	3V
Max/min detector on $C_{max}$ sampling frequency:	1 MHz
Max/min detector on $C_{max}$ sampling frequency:	100 MHz
Transducer-resonator parameters	As in table I

reaches a local minimum, the switch SW2 is opened, allowing the transducer to discharge through the inductor. When the voltage on  $C_{tran}$  is zero (the current in the inductor is maximal), the transducer is disconnected from the inductor by the switch SW2. The energy accumulated in the inductor is transferred to  $C_{res}$  through the diode  $D1$ .

Table II presents the numerical parameters of the circuit operation and the timing of the switch operation. The maximum/minimum detectors regularly sample the input quantity and search for a local maximum/minimum by analysing the last three sampled points (in practice, the maximum detection is done by analog signal processing [4]). Note that the characteristic time of the electromechanical energy conversion defined by the rate of the mobile mass motion is much larger than the time required for the energy transfer between  $C_{res}$  and  $C_{tran}$ . Hence, the detector detecting an  $I_L$  maximum operates at much higher frequency than the  $C_{tran}$  max/min detector.

The advantage of this model for our study is that its architecture is very close to the realistic circuit and it accounts for realistic parasitic effects such as losses in the flyback diodes. However, the presented model has two minor drawbacks for the theory validation. Firstly, it does not correspond exactly to the mathematical model described in Section II since it includes the diodes and considers a small finite time for the charging/discharging processes, and its dynamics may be slightly different from those described by the mathematical model. Secondly, the simulation time is long. These are the reasons why the idealised circuit of Fig. 2 is introduced as an intermediate validation step.

#### IV. MULTIPLE SCALES METHOD

The method of multiple scales (MSM) is an asymptotic method that is often applied for the analysis of weakly nonlinear oscillators [22], both autonomous and under external excitation. The idea behind this method is to present oscillations in a quasi-harmonic form and to find adjustments to oscillation characteristics, such as amplitude and phase, that result from the nonlinearity. The method is known to be an effective tool for a range of system, from the classical Duffing's oscillator [22] to voltage controlled oscillators [23] and recently was employed to study nonlinear vibrations of piezoelectric harvesters [24]. In this section, the application of the MSM to the e-VEH system is presented. More details about the standard implementation of the method can be found in [22].

### A. Standard Implementation of the Method

In (5), the dimensionless parameters  $\beta$ ,  $\kappa_0$ ,  $\nu_0$  and  $\alpha$  are relatively small with respect to unity. Since we consider a resonant harvester, we also introduce a small  $\sigma$  representing the external vibration frequency mismatch with the natural resonance frequency of the resonator:  $\Omega = 1 + \sigma$ . To emphasise the terms with small parameters, we introduce a small quantity  $\varepsilon$  and replace them by the following products:  $\beta = \varepsilon\tilde{\beta}$ ,  $\alpha = \varepsilon\tilde{\alpha}$ , and  $\sigma = \varepsilon\tilde{\sigma}$ . We also note the functions  $f_t$  are the product of the coefficients  $\kappa_0$  and  $\nu_0$  and dimensionless ratios containing  $y$  or  $y_{\max}$ , so we can also present  $\kappa_0 = \varepsilon\tilde{\kappa}_0$  and  $\nu_0 = \varepsilon\tilde{\nu}_0$ . In order to put them into the correct order of the small parameter  $\varepsilon$  in the method, we will note  $f_t = \varepsilon\tilde{f}_t$ . Thus,

$$y'' + 2\varepsilon\tilde{\beta}y' + y = \varepsilon\tilde{f}_t(y, y') + \varepsilon\tilde{\alpha}\cos(\tau + \varepsilon\tilde{\sigma}\tau + \theta_0). \quad (12)$$

The multiple scales method is a perturbation method that introduces the time scales  $T_k = \varepsilon^k\tau$ . In this case, the system dynamics defined by the process  $y(\tau)$  is now dependent on different time scales. The time derivatives are now given by

$$\frac{d}{d\tau} = D_0 + \varepsilon D_1, \quad \frac{d^2}{d\tau^2} = D_0^2 + 2\varepsilon D_0 D_1 \quad (13)$$

where  $D_k = \partial/\partial T_k$ ,  $k = 0, 1, \dots$ . For displacement  $y$ , a standard expansion for perturbation method is used:

$$y = y_0(T_0, T_1) + \varepsilon y_1(T_0, T_1). \quad (14)$$

Equation (12) now can be rewritten as follows:

$$\begin{aligned} & (D_0^2 + 2\varepsilon D_0 D_1)(y_0 + \varepsilon y_1) + 2\varepsilon\tilde{\beta}(D_0 + \varepsilon D_1) \\ & \times (y_0 + \varepsilon y_1) + y_0 + \varepsilon y_1 = \varepsilon\tilde{f}_t[y_0 + \varepsilon y_1, \\ & (D_0 + \varepsilon D_1)(y_0 + \varepsilon y_1)] + \varepsilon\tilde{\alpha}\cos(T_0 + \tilde{\sigma}T_1 + \theta_0). \end{aligned} \quad (15)$$

Collecting orders 0 and 1 of the parameter  $\varepsilon$ , and neglecting order 2 and higher, we obtain two equations

$$D_0^2 y_0 + y_0 = 0, \quad (16a)$$

$$\begin{aligned} D_0^2 y_1 + y_1 = & -2D_0 D_1 y_0 - 2\tilde{\beta} D_0 y_0 \\ & + \tilde{f}_t(y_0, D_0 y_0) + \tilde{\alpha}\cos(T_0 + \tilde{\sigma}T_1 + \theta_0). \end{aligned} \quad (16b)$$

In (15) the terms with  $\varepsilon$  in the arguments of  $\tilde{f}_t$  give second-order terms in the expansion of  $f_t$  over the powers of  $\varepsilon$ , hence we neglect them in (16b). The solution of (16a) is

$$y_0 = A(T_1)e^{iT_0} + c.c. = a(T_1)\cos(\tau + \varphi(T_1)) \quad (17)$$

where the slow complex amplitude  $A = (a/2)\exp(i\varphi)$  is expressed through the real slow amplitude  $a$ , and c.c. stands for the complex conjugate. In expression (16b), the function  $\tilde{f}_t(y_0, D_0 y_0)$  is a periodic function of  $T_0$  with period  $2\pi$  (as well as  $y_0$ ) and, therefore, we can use the Fourier series for the force  $\tilde{f}_t$ . Recalling that the system is high-Q resonant, we limit the series to the first harmonic

$$\tilde{f}_t(y_0, D_0 y_0) = \tilde{f}_0(a)$$

$$+ \tilde{a}_1(a)\cos(T_0 + \varphi) + \tilde{b}_1(a)\cos(T_0 + \varphi) \quad (18)$$

where  $\tilde{f}_0$ ,  $\tilde{a}_1$  and  $\tilde{b}_1$  are the following coefficients of the Fourier series:

$$\begin{aligned} \tilde{f}_0(a) &= \frac{1}{2\pi} \int_0^{2\pi} \tilde{f}_t(a\cos\theta, -a\sin\theta) d\theta \\ \tilde{a}_1(a) &= \frac{1}{\pi} \int_0^{2\pi} \tilde{f}_t(a\cos\theta, -a\sin\theta) \cos(\theta) d\theta \\ \tilde{b}_1(a) &= \frac{1}{\pi} \int_0^{2\pi} \tilde{f}_t(a\cos\theta, -a\sin\theta) \sin(\theta) d\theta. \end{aligned} \quad (19)$$

Equivalently, in the complex representation

$$\tilde{f}_t(y_0, D_0 y_0) = \tilde{f}_0(a) + [\tilde{c}_1(a)e^{iT_0+i\varphi} + c.c.] \quad (20)$$

where complex  $\tilde{c}_1$  is expressed through real  $\tilde{a}_1$  and  $\tilde{b}_1$

$$\tilde{c}_1(a) = (\tilde{a}_1(a) - i\tilde{b}_1(a))/2. \quad (21)$$

After the solution for  $y_0$  is substituted into (16b), we collect the terms that contain  $\exp(iT_0)$  since they lead to linear resonance of the undamped system. Equation (16b) yields one equation to find  $y_1$  and one equation for complex  $A(T_1)$ :

$$D_0^2 y_1 + y_1 = \tilde{f}_0, \quad (22a)$$

$$\begin{aligned} -2i\dot{A}e^{iT_0} - 2\tilde{\beta}iAe^{iT_0} + \tilde{c}_1(a)e^{iT_0+i\varphi} \\ + \tilde{\alpha}/2e^{i(T_0+\tilde{\sigma}T_1+\theta_0)} + c.c. = 0. \end{aligned} \quad (22b)$$

From expression (22a), it follows that  $y_1 = \tilde{f}_0$  and, as a consequence,  $\varepsilon y_1$  represents the average (zero frequency) shift of the mobile mass displacement due to the transducer force. Let us denote for convenience:

$$y_{av} = \varepsilon y_1 = \varepsilon\tilde{f}_0. \quad (23)$$

Therefore, the total solution will take the form

$$y(\tau) = y_0 + \varepsilon y_1 = y_{av} + a\cos(\tau + \varphi). \quad (24)$$

Dividing (22b) into real and imaginary parts, one obtains equations for the slow amplitude  $a$  and the phase  $\psi = \tilde{\sigma}T_1 + \theta_0 - \varphi$

$$\begin{aligned} \dot{a} = & -\tilde{\beta}a - \frac{\tilde{b}_1(a)}{2} + \frac{\tilde{\alpha}}{2}\sin\psi, \\ a\dot{\psi} = & a\tilde{\sigma} + \frac{\tilde{a}_1(a)}{2} + \frac{\tilde{\alpha}}{2}\cos\psi. \end{aligned} \quad (25)$$

It is relevant to note that this system of differential equations provides information about transient dynamics of the system, and allows one to explore the dynamics around multiple stable points and identify different possible stable modes.

Let us find the steady-state solution  $a_0$  and  $\psi_0$  from the condition  $\dot{a} = 0$  and  $\dot{\psi} = 0$ . For the phase  $\psi_0$  one obtains a set of equations

$$\begin{aligned} \frac{\tilde{\alpha}}{2}\sin\psi_0 = & \tilde{\beta}a_0 + \frac{\tilde{b}_1(a_0)}{2}, \\ \frac{\tilde{\alpha}}{2}\cos\psi_0 = & -a_0\tilde{\sigma} - \frac{\tilde{a}_1(a_0)}{2}. \end{aligned} \quad (26)$$

The equation for the amplitude  $a_0$  can now be found from (26)

$$\frac{\tilde{\alpha}^2}{4} = \left( \tilde{\beta}a_0 + \frac{\tilde{b}_1(a_0)}{2} \right)^2 + \left( a_0\tilde{\sigma} + \frac{\tilde{a}_1(a_0)}{2} \right)^2. \quad (27)$$

Expressions (24), (26) and (27) define the steady-state response of the nonlinear oscillator (5) to the external driving and the nonlinear force  $f_t$ . Note that by multiplying both sides of (27) by  $\varepsilon^2$  we can rewrite this equation with the original values of  $\alpha$ ,  $\beta$  and  $\sigma$  in the same form.

The steady-state solution therefore is

$$y(\tau) = y_{av,0} + a_0 \cos((1 + \sigma)\tau + \theta_0 - \psi) \quad (28)$$

where we have used the index ‘0’ to emphasize that  $y_{av}$ ,  $a$  and  $\psi$  are steady-state characteristics.

### B. Stability of Steady-State Solutions

Formally,  $\mathbf{x}_0 = (a_0, \psi_0)$  is a fixed point of the set (25). To analyse its stability, we introduce small perturbations  $a_1(T_1)$  and  $\psi_1(T_1)$  to  $a_0$  and  $\psi_0$  and substitute  $a(T_1) = a_0 + a_1$  and  $\psi(T_1) = \psi_0 + \psi_1$  into (25). The linearised system describing the evolution of  $\mathbf{x}_1 = (a_1, \psi_1)$  has the following form:

$$\begin{pmatrix} \dot{a}_1 \\ \dot{\psi}_1 \end{pmatrix} = \begin{pmatrix} -\tilde{\beta} - \frac{\tilde{b}'_1}{2} & \frac{\tilde{\alpha}}{2} \cos \psi_0 \\ \frac{1}{a_0} \left( \tilde{\sigma} + \frac{\tilde{a}'_1}{2} \right) & -\frac{\tilde{\alpha}}{2a_0} \sin \psi_0 \end{pmatrix} \begin{pmatrix} a_1 \\ \psi_1 \end{pmatrix} \quad (29)$$

where the matrix is in fact the Jacobian  $J(\mathbf{x})$  obtained from (25) and taken at  $\mathbf{x} = \mathbf{x}_0$ .

Thus, stability of the fixed point  $\mathbf{x}_0 = (a_0, \psi_0)$  is defined by the eigenvalues of the matrix in (29). According to the Routh-Hurwitz criterion, the point  $(a_0, \psi_0)$  is stable if the following conditions are fulfilled:

$$\begin{aligned} 2\tilde{\beta} + \frac{\tilde{b}'_1}{2} + \frac{\tilde{b}_1}{2a_0} &> 0 \\ \left( \tilde{\beta} + \frac{\tilde{b}'_1}{2} \right) \left( \tilde{\beta} + \frac{\tilde{b}_1}{2a_0} \right) + \left( \tilde{\sigma} + \frac{\tilde{a}'_1}{2} \right) \left( \tilde{\sigma} + \frac{\tilde{a}_1}{2a_0} \right) &> 0. \end{aligned} \quad (30)$$

If the above conditions are not fulfilled, the orbit that is defined by these  $a_0$  and  $\psi_0$  is unstable (a saddle orbit). The above stability condition is necessary, but not sufficient. We note here that for nonlinear oscillators, it is very typical that the increase of the external force amplitude or other parameters leads to bifurcations of previously stable orbits and eventually, to irregular, chaotic behavior. Though these dynamics are beyond the scope of this paper, the results obtained by the MSM can be used in a further analysis. We report the results of this research in [25].

### C. Improving Accuracy for the Estimation of the Zeroth Harmonic

The described above algorithm works very well if the average shift  $y_{av,0} = \varepsilon y_1$  is relatively small compared to the amplitude  $a_0$  of oscillations (see the discussion on the comparison between the model simulations and the theory in the next section). However, for the gap-closing transducer whose force is expressed by (8) the constant shift of oscillations can be large and even larger than  $a_0$  [18]. This leads to a non-negligible error in  $y_{av}$  provided

by the standard implementation of the MSM that we described in Section IV.A. This error appears from the underestimation of the force  $\tilde{f}_t$  that can be relatively large and that produces the average shift of  $y(\tau)$ .

In order to accurately incorporate this effect into the model, we can use the solution (24) when presenting  $\tilde{f}_t$  as a Fourier expansion. Since the transducer forces (8) depend on the maximum displacement that we define as  $y_{\max} = y_{av} + a$ , the Fourier coefficients will be the functions of both,  $y_{av}$  and  $a$ :  $\tilde{f}_0(y_{av}, a)$ ,  $\tilde{a}_1(y_{av}, a)$  and  $\tilde{b}_1(y_{av}, a)$ . Practically, it means that the Fourier expansion is carried out for  $\tilde{f}_t(y_0 + \varepsilon y_1)$  in (16b). Equations (26) and (27) are rewritten as

$$\begin{aligned} \frac{\tilde{\alpha}}{2} \sin \psi_0 &= \tilde{\beta}a_0 + \frac{\tilde{b}_1(y_{av,0}, a_0)}{2}, \\ \frac{\tilde{\alpha}}{2} \cos \psi_0 &= -a_0\tilde{\sigma} - \frac{\tilde{a}_1(y_{av,0}, a_0)}{2} \end{aligned} \quad (31)$$

$$\frac{\tilde{\alpha}^2}{4} = \left( \tilde{\beta}a_0 + \frac{\tilde{b}_1(y_{av,0}, a_0)}{2} \right)^2 + \left( a_0\tilde{\sigma} + \frac{\tilde{a}_1(y_{av,0}, a_0)}{2} \right)^2. \quad (32)$$

These equations have three unknown variables:  $y_{av,0}$ ,  $a_0$  and  $\psi_0$ . One more equation is required to obtain a self-consistent system and it is obtained from (23) for the average shift  $y_{av,0}$ , where we assume that  $\tilde{f}_0$  depends on  $a_0$  and on  $y_{av,0}$  itself

$$y_{av,0} = \tilde{f}_0(y_{av,0}, a_0). \quad (33)$$

Solving the four expressions given by (31), (32) and (33), we find  $a_0$  and  $y_{av,0}$  and  $\psi_0$  to be used in solution (28).

Finally, we briefly note how we derived a criterion similar to (30) to obtain the necessary condition for stability. There are three actual variables in the system: the amplitude  $a$ , the phase  $\psi$  and the shift  $y_{av}$ . The evolution of  $a$  and  $\psi$  is given by (25) with the difference that now  $\tilde{a}_1$  and  $\tilde{b}_1$  are functions of  $a$  and  $y_{av}$ . The third equation that determines the evolution of  $y_{av}$  is obtained by differentiating expression (33). Therefore, the dynamics of the variable are given by the equations

$$\begin{aligned} \dot{a} &= -\tilde{\beta}a - \frac{\tilde{b}_1(y_{av}, a)}{2} + \frac{\tilde{\alpha}}{2} \sin \psi = F(a, \psi, y_{av}), \\ \dot{\psi} &= \tilde{\sigma} + \frac{\tilde{a}_1(y_{av}, a)}{2a} + \frac{\tilde{\alpha}}{2a} \cos \psi = G(a, \psi, y_{av}), \\ \dot{y}_{av} &= \frac{1}{1 - \partial \tilde{f}_0 / \partial y_{av}} \frac{\partial \tilde{f}_0}{\partial a} \dot{a} = H(a, \psi, y_{av}). \end{aligned} \quad (34)$$

Now  $\mathbf{x}_0 = (a_0, \psi_0, y_{av,0})$  is a fixed point of (34). Similarly to Section IV.B, the small perturbations  $\mathbf{x}_1 = (a_1, \psi_1, y_{av,1})$  from  $\mathbf{x}_0$  are introduced into (34). The dynamics of the perturbations are defined by the equation

$$\dot{\mathbf{x}}_1^T = J(\mathbf{x})|_{\mathbf{x}=\mathbf{x}_0} \mathbf{x}_1^T \quad (35)$$

where the Jacobian  $J(\mathbf{x})$  is obtained from (34) and taken at  $\mathbf{x}_0 = (a_0, \psi_0, y_{av,0})$ . In this case we obtain a cubic polynomial to find the eigenvalues of  $J$  and we state the same necessary condition: in order for a solution to be stable, all real parts of the eigenvalues must be negative.

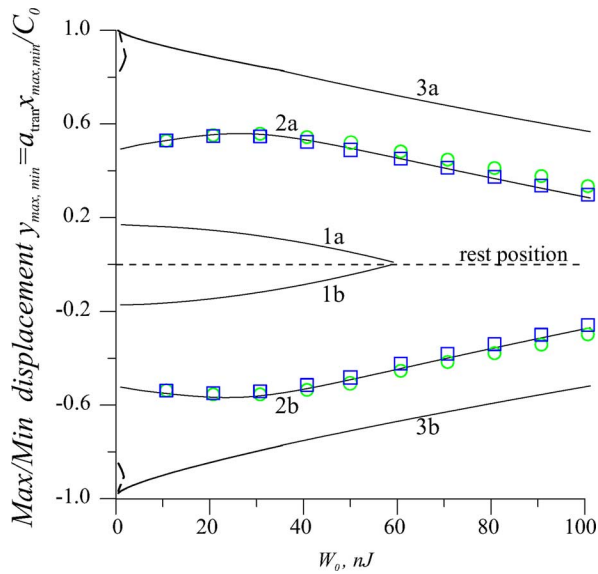


Fig. 4. Area overlap transducer: the envelope (maximum and minimum values) of oscillations as a function of the energy  $W_0$  at  $A_{\text{ext}} = 5 \text{ m/s}^2$  (line 1),  $A_{\text{ext}} = 15 \text{ m/s}^2$  (line 2) and  $A_{\text{ext}} = 25 \text{ m/s}^2$  (line 3). Marks ‘a’ and ‘b’ denote the maximum and minimum values of the displacement respectively. The zero displacement or the rest position is shown by the dashed line. Squares show the envelope obtained from VHDL-AMS simulations of the idealised model from Fig. 2 while circles show the simulations of the realistic model from Fig. 3.

## V. STEADY-STATE OSCILLATIONS: PARTICULAR EXAMPLES OF THE TRANSDUCER

### A. Steady-State Oscillations

Let us investigate the two particular cases of the transducer. For the area overlap transducer with  $f_t$  defined as (6), the coefficients of the Fourier series are

$$\begin{aligned} f_0(a) &= \frac{\kappa_0}{2(1-a)\sqrt{1-a^2}} \\ a_1(a) &= -\frac{\kappa_0 a}{(1-a)(1-a^2)^{1/2}}, \quad b_1(a) = \frac{2\kappa_0}{\pi(1-a)} \end{aligned} \quad (36)$$

and they are substituted into (26) and (27). The envelope of oscillations (i.e., the maximum  $y_{\text{max}} = y_{\text{av},0} + a_0$  and the minimum  $y_{\text{min}} = y_{\text{av},0} - a_0$  values of the oscillation) as a function of the energy  $W_0$  is shown in Fig. 4 at three different values of the external acceleration  $A_{\text{ext}}$ . Note a slight asymmetry of the envelope: there is a non-zero average shift of oscillations that becomes more pronounced at  $W_0 > 50 \text{ nJ}$ .

At large accelerations  $A_{\text{ext}}$  and small energies  $W_0$  when the oscillations of the resonator are large the system is multistable: there are three coexisting solutions of (27) with one of them unstable according to the criterion (30). Such an unstable solution can never be observed in numerical simulations of the original system (5) or in a realistic device. Alternatively, we can fix  $W_0$  and vary  $A_{\text{ext}}$ , to see a bifurcation diagram of the parameter  $A_{\text{ext}}$  in detail (Fig. 5). The two solutions, marked by 1 and 3 in Fig. 5, are stable orbits that one can observe in numerical simulations by setting different initial conditions as is shown, while curve 2 shows the unstable branch.

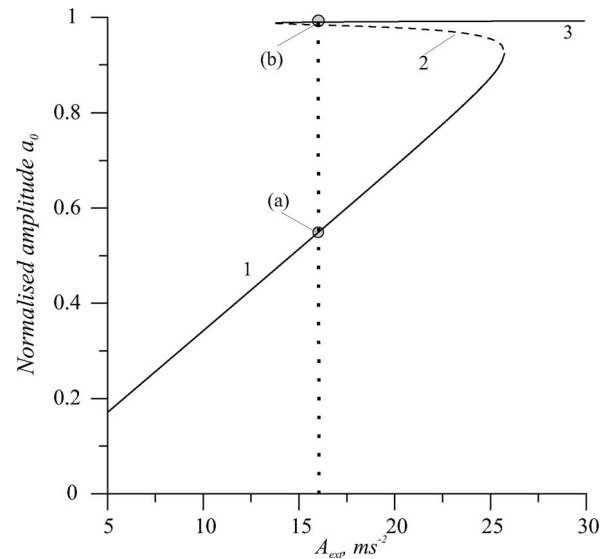


Fig. 5. Area overlap transducer: bifurcation diagram versus  $A_{\text{ext}}$  (at the fixed energy  $W_0 = 375 \text{ pJ}$ ) showing two branches that correspond to stable orbits (solid lines) and a branch that correspond to an unstable orbit (dashed line). Over a range of the bifurcation parameter  $A_{\text{ext}}$ , the two stable orbits coexist. Particular examples of oscillations that correspond to the two stable branches at  $A_{\text{ext}} = 16 \text{ m/s}^2$  marked (a) and (b) are shown in Fig. 7.

In the case of the gap-closing transducer, the coefficients of the first Fourier harmonics are

$$\begin{aligned} f_0(y_{\text{av}}, a) &= \frac{\nu_0}{2(1-y_{\text{av}}-a)}, \quad a_1(y_{\text{av}}, a) = 0, \\ b_1(y_{\text{av}}, a) &= \frac{2\nu_0}{\pi(1-y_{\text{av}}-a)} \end{aligned} \quad (37)$$

and they are substituted into (31), (32) and (33) in order to obtain a more accurate solution. The envelope of oscillations as a function of the energy  $W_0$  for the gap-closing transducer is shown in Fig. 6 at different values of the external acceleration  $A_{\text{ext}}$ . In this case the asymmetry of the envelope is stronger: there are such energies  $W_0$  that both, maximum  $y_{\text{av},0} + a_0$  and minimum  $y_{\text{av},0} - a_0$ , are above the rest (zero) position.

Note that in this case, there also exist multiple solutions for  $a_0$  and  $\psi_0$  at certain  $W_0$  and  $A_{\text{ext}}$ , i.e., formally this system is also multistable. However, the other roots of (27) are greater than unity and, as follows from the expressions (8), they lie in the ‘‘unphysical’’ region for this system. The only physical solution is stable according to the criterion described in IV.C.

### B. Comparison With VHDL-AMS/Eldo Modelling

Numerical simulation was carried out with the VHDL-AMS/Eldo models described in Section III. Firstly, we compare the simulations with the analytically calculated envelope of oscillations in Figs. 4 and 6 for the two transducers. The results of the VHDL-AMS/Eldo simulations shown by squares for the idealised model (from Fig. 2) and by circles for the realistic model (from Fig. 3). While the idealised model agrees very well with the theory for the both transducers, there is a slight discrepancy with the realistic model. We recall that the realistic model includes certain parasitic effects such as losses on the diodes. Therefore, the realistic circuit does not extract mechanical energy from the resonator as effectively as the idealised circuit.

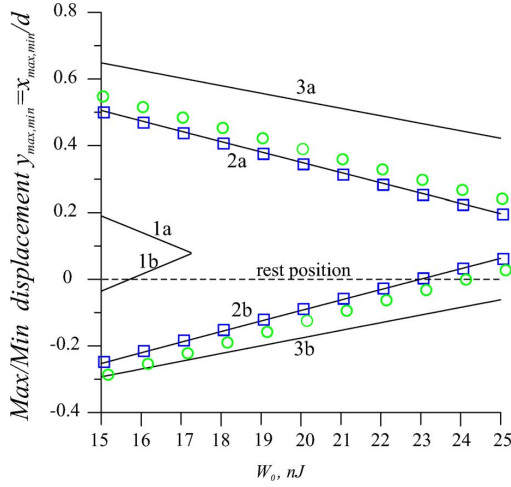


Fig. 6. Gap-closing transducer: the envelope (maximum and minimum values) of oscillations as a function of  $W_0$  at  $A_{\text{ext}} = 3 \text{ m/s}^2$  (line 1),  $A_{\text{ext}} = 5 \text{ m/s}^2$  (line 2) and  $A_{\text{ext}} = 7 \text{ m/s}^2$  (line 3). Marks ‘a’ and ‘b’ denote the maximum and minimum values of the displacement respectively. The zero displacement or the rest position is shown by the dashed line. Squares show the envelope obtained from VHDL-AMS simulations of the idealised model from Fig. 2 while circles show the simulations of the realistic model from Fig. 3.

This causes the amplitude of vibrations in the resonator to be slightly larger than it could be in the ideal system.

Fig. 7 presents the simulation results for the normalised displacement  $y(\tau)$  obtained with different initial conditions  $y(0)$  and  $y'(0)$ . Numerical simulations agree with the predictions of the MSM: the amplitude of the waveform 7(a) corresponds to the point (a) on the lower branch of the bifurcation diagram 5 while the amplitude in Fig. 7(b) corresponds to the upper branch of that diagram and is marked as (b). We note that in this case the observed dynamics are somewhat similar to those of the Duffing oscillator under a harmonic excitation.

### C. Necessary Conditions to Start Oscillations

From Figs. 4 and 6, it is clearly seen that there exist values of the circuit control parameters  $W_0$  and the acceleration  $A_{\text{ext}}$  for which there are no positive values of steady-state amplitude  $a_0$  (see, for example, how the lines marked by 1 cross the horizontal axis in Figs. 4 and 6). Since  $a_0$  denotes the amplitude of oscillations, it has a physical meaning if it is positive. We can summarise this as follows. At a given  $W_0$  there exists  $A_{\text{ext}}^{\text{min}}$  such that the system oscillates if  $A_{\text{ext}} > A_{\text{ext}}^{\text{min}}$ . And vice versa, at a given  $A_{\text{ext}}$  there exist  $W_0^{\text{max}}$  such that the system oscillates if  $W_0 < W_0^{\text{max}}$ . The existence of a minimal  $A_{\text{ext}}$  was discovered in a behavioral model in [18]. If this condition on  $W_0$  and  $A_{\text{ext}}$  is not fulfilled, the operating mode of the e-VEH is irregular and uncontrollable in a realistic context.

Firstly we give a detailed example for the area overlap transducer (6) since the expression for  $A_{\text{ext}}^{\text{min}}$  and  $W_0^{\text{max}}$  can be obtained for it in a very simple form. Let us assume that  $a_0 = 0$  in (27). This condition will provide us with a *necessary condition* to start oscillations. For the dimensionless parameters one obtains a simple expression

$$\alpha^2 = a_1^2(a_0)|_{a_0=0} + b_1^2(a_0)|_{a_0=0} \quad (38)$$

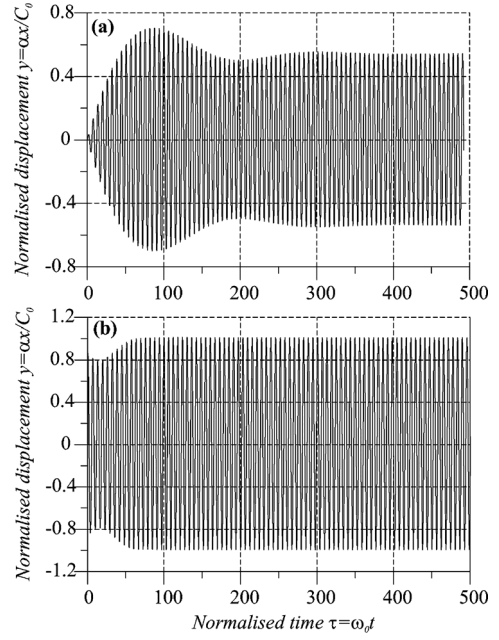


Fig. 7. Area overlap transducer: coexisting oscillations at  $W_0 = 375 \text{ pJ}$  and  $A_{\text{ext}} = 16 \text{ m/s}^2$ . Two waveforms correspond to the lower and upper branches at the points marked as (a) and (b) in Fig. 5.

Substituting (36) into (38), one finds the relations between the normalised acceleration  $\alpha^{\text{min}}$  (or  $A_{\text{ext}}^{\text{min}}$ ) and given normalised circuit parameters  $\kappa_0$  (or  $W_0$ ):

$$\alpha^{\text{min}} = 2\kappa_0/\pi, \quad A_{\text{ext}}^{\text{min}} = \frac{2\alpha_{\text{tran}}W_0}{\pi m C_0} \quad (39)$$

The inverse expressions that relate the boundary values of the circuit control parameter  $W_0^{\text{max}}$  with some given external acceleration  $A_{\text{ext}}$  are easily obtained from the above. Let us give a numerical example: what maximal value of  $W_0$  should be fixed on the transducer to obtain oscillations at  $A_{\text{ext}} = 5 \text{ m/s}^2$ ? From (39) it follows that  $W_0^{\text{max}} = 59 \text{ nJ}$ . This corresponds exactly to the point in Fig. 4 where the envelope disappears (this  $A_{\text{ext}}$  corresponds to the lines 1a and 1b). Therefore, no oscillations are possible if  $W_0 > W_0^{\text{max}}$ .

For the gap-closing transducer one solves the set of (32) and (33):

$$\begin{aligned} \alpha^2 &= a_1^2(y_{av,0}, a_0)|_{a_0=0} + b_1^2(y_{av,0}, a_0)|_{a_0=0} \\ y_{av,0} &= f_0(y_{av,0}, a_0)|_{a_0=0} \end{aligned} \quad (40)$$

and finds the required starting parameter together with the resulting average shift. For example, at  $A_{\text{ext}} = 3 \text{ m/s}^2$ ,  $W_0^{\text{max}} = 17.4 \text{ nJ}$ , which corresponds to the point in Fig. 6 where the envelope disappears (this  $A_{\text{ext}}$  corresponds to the lines 1a and 1b).

Now let us illustrate the presence of the boundary parameters required for oscillations in simulations of the behavioral VHDL-AMS model. Fig. 8(a) shows a slowly growing ramp of acceleration (in  $\text{ms}^{-2}$ ) as a function of the normalised time  $\tau$ . At this  $A_{\text{ext}}$ , the displacement  $y$  is obtained as a function of time, Fig. 8(b). Below the boundary value of  $A_{\text{ext}}^{\text{min}}$ , the dynamics of the system are irregular with many local maxima detected in one period of oscillations (Fig. 8(c)). Only above this threshold, one



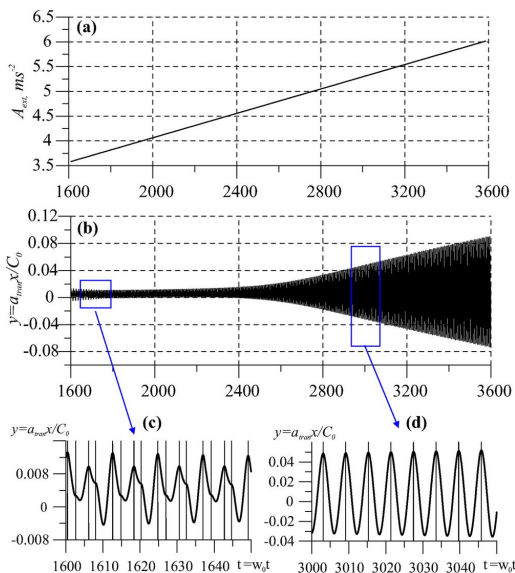


Fig. 8. Area overlap transducer: (a) slowly growing ramp of  $A_{\text{ext}}$  (the envelope of the external oscillations) and (b) corresponding displacement of the harvester as functions of normalised time. Two magnified waveforms show the case when no regular oscillations are observed (c) and when harmonic oscillations have started (d).

can observe harmonic oscillations with one maximum detected during one period of oscillations (Fig. 8(d)).

## VI. DISCUSSION AND CONCLUSIONS

In this section we give a discussion of our theoretical approach, highlight the difference with the analytical tool from [14] and point out the immediate practical value of the results for design of e-VEHs.

The MSM is known as a powerful and flexible method for analysis of nonlinear systems. The two main practical benefits that we obtained from the theory are

- It allowed us to obtain equations that fully describe the oscillations in the system. Now, for any set of parameters, one can calculate the resulting oscillation and therefore converted power. It also gives the initial analysis of stability. The results obtained with this method have been used for further stability analysis in [25], [26]. Therefore, for the gap-closing transducer, based on the results presented in this paper, we define all possible dynamics of the system and find values of the system parameters where the system displays regular harmonic oscillations. Practically, this is very important since the conditioning circuit can operate correctly and effectively only if this is the case.
- Another conclusion that immediately follows from the method is the existence of ‘boundary’ values for the acceleration amplitude  $A_{\text{ext}}$  and the energy  $W_0$  required to start oscillations in the resonator. The method yields a simple way to calculate these boundary values. This is also an important result from a practical standpoint: knowing parameters of the environment, one can optimize the design parameter  $W_0$ . For the area overlap transducer, the expressions that give the boundary values for  $A_{\text{ext}}$  and  $W_0$  are very simple.

In addition, the method allows one to expand it to the case of different nonlinearities. This will allow the exploration of nonlinear effects that seem to be very promising for widening the frequency response of the system [27]–[29].

The limitations of the method follow from limitations that are inherit in perturbation techniques. Firstly, there is a very general condition for all perturbation methods that nonlinearities should be relatively small (this ‘smallness’ can be easily established in the normalised dimensionless equation by comparing the parameters of the nonlinear terms with unity). In our case, this is equivalent to stating that the method will work while oscillations can be described as quasi-harmonic. As is shown by the simulations based on the VHDL-AMS model, this is typically the case for the system over a wide range of parameters. Secondly, despite the flexibility of the MSM, it demands that nonlinear terms should be arranged accurately with respect to the order of the small parameter  $\varepsilon$ . We note that for the gap-closing transducer we have overcome this difficulty by introducing a modification of the standard MSM implementation where we compensate an error that appeared due to the large constant shift  $y_{av,0}$ .

We also point out that all analytical results are verified by simulations of a realistic behavioral model carried out with VHDL-AMS/Eldo simulators.

## REFERENCES

- [1] S. Roundy, P. Wright, and K. Pister, “Micro-electrostatic vibration-to-electricity converters,” in *Proc. 2002 ASME Int. Mechanical Engineering Congr.*, Nov. 2002, pp. 487–496.
- [2] G. Despesse, T. Jager, J. J. Chaillout, J. M. Leger, A. Vassilev, S. Bascour, and B. Charlot, “Fabrication and characterization of high damping electrostatic micro devices for vibration energy scavenging,” in *Proc. DTIP MEMS MOEMS Conf.*, 2005, pp. 386–390.
- [3] P. Basset, D. Galayko, A. Paracha, F. M. A. Dudka, and T. Bourouina, “A batch-fabricated and electret-free silicon electrostatic vibration energy harvester,” *J. Micromech. Microeng.*, vol. 19, no. 11, p. 115025, Nov. 2009.
- [4] S. Meninger, J. Mur-Miranda, R. Amiratharajah, A. Chandrakasan, and J. Lang, “Vibration-to-electric energy conversion,” *IEEE Trans. Very Large Scale Integr. (VLSI) Syst.*, vol. 9, no. 1, pp. 64–76, 2001.
- [5] B. C. Yen and J. H. Lang, “A variable-capacitance vibration-to-electric energy harvester,” *IEEE Trans. Circuits Syst. I, Reg. Papers*, vol. 53, pp. 288–295, 2006.
- [6] E. Torres and G. Rincón-Mora, “Electrostatic energy-harvesting and battery-charging CMOS system prototype,” *IEEE Trans. Circuits Syst. I, Reg. Papers*, vol. 56, no. 9, pp. 1938–1948, 2009.
- [7] M. Kiziroglou, C. He, and E. Yeatman, “Flexible substrate electrostatic energy harvester,” *Electron. Lett.*, vol. 46, no. 2, pp. 166–167, 2010.
- [8] E. O. Torres and G. A. Rincón-Mora, “Electrostatic energy-harvesting and battery-charging CMOS system prototype,” *IEEE Trans. Circuits Syst. I, Reg. Papers*, vol. 56, no. 9, pp. 1938–1948, Sep. 2009.
- [9] Y. Naruse, N. Matsubara, K. Mabuchi, M. Izumi, and S. Suzuki, “Electrostatic micro power generation from low-frequency vibration such as human motion,” *J. Micromech. Microeng.*, vol. 19, p. 094002, 2009.
- [10] D. Hoffmann, B. Folkmer, and Y. Manoli, “Fabrication, characterization and modelling of electrostatic micro-generators,” *J. Micromech. Microeng.*, vol. 19, p. 094001, 2009.
- [11] W. Ma, R. Zhu, L. Rufer, Y. Zohar, and M. Wong, “An integrated floating-electrode electric microgenerator,” *J. Microelectromech. Syst.*, vol. 16, no. 1, pp. 29–37, 2007.
- [12] P. Mitcheson, E. Yeatman, G. Rao, A. Holmes, and T. Green, “Energy harvesting from human and machine motion for wireless electronic devices,” *Proc. IEEE*, vol. 96, no. 9, pp. 1457–1486, 2008.
- [13] R. Guillemet, P. Basset, D. Galayko, and T. Bourouina, “Design optimization of an out-of-plane gap-closing electrostatic vibration energy harvester (VEH) with a limitation on the output voltage,” *Analog Integr. Circuits Signal Process.*, pp. 1–9, 2011.

- [14] D. Galayko and P. Basset, "A general analytical tool for the design of vibration energy harvesters (VEHs) based on the mechanical impedance concept," *IEEE Trans. Circuits Syst. I, Reg. Papers*, no. 99, pp. 299–311, 2011.
- [15] B. Stark, P. Mitcheson, P. Miao, T. Green, E. Yeatman, and A. Holmes, "Converter circuit design, semiconductor device selection and analysis of parasitics for micropower electrostatic generators," *IEEE Trans. Power Electron.*, vol. 21, no. 1, pp. 27–37, 2006.
- [16] A. Paracha, P. Basset, D. Galayko, F. Marty, and T. Bourouina, "A silicon MEMS DC/DC converter for autonomous vibration-to-electrical-energy scavenger," *IEEE Electron Device Lett.*, vol. 30, no. 5, pp. 481–483, 2009.
- [17] P. Miao, P. Mitcheson, A. Holmes, E. Yeatman, T. Green, and B. Stark, "MEMS inertial power generators for biomedical applications," *Microsystem Technol.*, vol. 12, no. 10, pp. 1079–1083, 2006.
- [18] D. Galayko, R. Guillemet, A. Dudka, and P. Basset, "Comprehensive dynamic and stability analysis of electrostatic vibration energy harvester (E-VEH)," in *Proc. 2011 Int. Conf. Solid-State Sensors, Actuators and Microsystems (TRANSDUCERS)*, 2011, pp. 2382–2385.
- [19] J. Miranda, "Electrostatic Vibration-to-Electric Energy Conversion," Ph.D. Dissertation, Massachusetts Institute of Technology, Cambridge, MA, Feb. 2003.
- [20] W. Tang, T. Nguyen, M. Judy, and R. Howe, "Electrostatic-comb drive of lateral polysilicon resonators," *Sens. Actuators A: Phys.*, vol. 21, no. 1–3, pp. 328–331, 1990.
- [21] F. Pêcheux, C. Lallement, and A. Vachoux, "Vhdl-ams and verilog-ams as alternative hardware description languages for efficient modeling of multidiscipline systems," *IEEE Trans. Computer-Aided Design Integr. Circuits Syst.*, vol. 24, no. 2, pp. 204–225, 2005.
- [22] A. Nayfeh, *Introduction to Perturbation Techniques*. New York: Wiley, 1993.
- [23] A. Buonomo and A. Lo Schiavo, "On the theory of quadrature oscillations obtained through parallel LC VCOs," *IEEE Trans. Circuits Syst. I, Reg. Papers*, vol. 57, pp. 2509–2519, 2010.
- [24] M. A. Karami and D. J. Inman, "Equivalent damping and frequency change for linear and nonlinear hybrid vibrational energy harvesting systems," *J. Sound Vibration*, vol. 330, pp. 5583–5597, 2011.
- [25] E. Blokhina, D. Galayko, R. Wade, P. Basset, and O. Feely, "Bifurcations and chaos in electrostatic vibration energy harvesters," in *Proc. IEEE Int. Symp. Circuits Syst.*, Seoul, Korea, May 20–24, 2012, pp. 397–400, 2012.
- [26] E. O'Riordan, P. Harte, E. Blokhina, D. Galayko, and O. Feely, "Bifurcation scenarios in electrostatic vibration energy harvesters," in *Proc. 2012 Int. Con. Nonlinear Dynamics of Electron. Syst.*, Wolfenbittel, Germany, Jul. 11–13, 2012, pp. 34–37.
- [27] F. Cottone, L. Gammaioni, and H. Vocca, "Nonlinear energy harvesting," *Phys. Rev. Lett.*, vol. 102, p. 08061, 2009.
- [28] S. Stanton, C. McGehee, and B. Mann, "Nonlinear dynamics for broadband energy harvesting: Investigation of a bistable piezoelectric inertial generator," *Physica D: Nonlinear Phenomena*, vol. 239, no. 10, pp. 640–653, 2010.
- [29] L. Blystad, E. Halvorsen, and S. Husa, "Piezoelectric MEMS energy harvesting systems driven by harmonic and random vibrations," *IEEE Trans. Ultrason., Ferroelectr. Freq. Contr.*, vol. 57, no. 4, pp. 908–919, 2010.



**Elena Blokhina** (S'05–M'06) received the M.Sc. and Ph.D. degrees in physics from Saratov State University, Russia, in 2002 and 2005, respectively.

From 2005 to 2007, she was a Research Scientist at Saratov State University, where she worked in the area of analysis and modeling of microwave electron devices. Since 2007, she has been with the Circuits and Systems Research Group, University College Dublin, Ireland, and is currently a research manager. Her research interests include nonlinear dynamics and physics of oscillations and waves and their application to the analysis and control of MEMS and energy harvesters.



**Dimitri Galayko** (M'12) graduated from Odessa State Polytechnic University, Ukraine, in 1998, he received the M.S. degree from Institut of Applied Sciences of Lyon (INSA), Lyon, France, in 1999. He made his Ph.D. thesis in the Institute of Microelectronics and Nanotechnologies (IEMN, Lille, France) and received the Ph.D. degree from the University Lille-I in 2002. The topic of his Ph.D. dissertation was the design of microelectromechanical silicon filters and resonators for radiocommunications.

Since 2005 he is an Associate Professor in University Paris-VI (Pierre et Marie Curie), France, in the LIP6 laboratory. His research interests include study, modeling and design of nonlinear integrated circuits for sensor interface and for mixed-signal applications.



**Philippe Basset** received the engineering diploma in electronics from ISEN Lille, France, in 1997, and the M.Sc. and Ph.D. degrees from the University of Lille at the Institute of Electronic, Microelectronic and Nanotechnologies (IEMN), France, in 1999 and 2003, respectively.

In 2004, he was a post-doc in Garry Fedder's group at Carnegie Mellon University, Pittsburgh, PA. In 2005 he joined ESIEE Paris at the University Paris-Est, France, where he is currently an Associate Professor. His research interests are in the area of

MEMS sensors and actuators, and micropower sources for autonomous MEMS.

Dr. Basset received a doctoral fellowship from CNRS for 2000–2003 and in 2005 a 3-year young researcher grant from the French Research Agency (ANR) to work on energy harvesting using micro- and nano- technologies.



**Orla Feely** (S'85–M'86–SM'00–F'09) received the B.E. degree in electronic engineering from University College Dublin (UCD), Ireland, in 1986, and the M.S. and Ph.D. degrees in electrical engineering from the University of California, Berkeley, in 1990 and 1992.

She joined UCD in 1992 and is currently a Professor in the School of Electrical, Electronic and Communications Engineering. Her research interests lie in the area of nonlinear dynamics of electronic circuits.

Prof. Feely is a Fellow of the IEEE, in recognition of her contributions to nonlinear discrete-time circuits and systems, and of Engineers Ireland. She received the Best Paper Awards of the International Journal of Circuit Theory and Applications, 2007, and the European Conference on Circuit Theory and Design, 1997. Her Ph.D. thesis won the D. J. Sakrison Memorial Prize for outstanding and innovative research, awarded annually by the Department of Electrical Engineering and Computer Science, U. C. Berkeley. She serves/has served on the Editorial Boards of the IEEE TRANSACTIONS ON CIRCUITS AND SYSTEMS—I: REGULAR PAPERS, the *International Journal of Circuit Theory and Applications* and the *IEICE Journal of Nonlinear Theory and its Applications*, and as Chair of the IEEE Technical Committee on Nonlinear Circuits and Systems.